Special Feature: Sensors

Development of Inertial Force Sensing System for Control of Partner Robot

Yutaka Nonomura, Motohiro Fujiyoshi and Hisayoshi Sugihara

■ABSTRACT‖ An inertial force sensing system for control of a partner robot was developed. We named this system MOST (MOtion Sensing Technology). MOST provides a set of the true posture angles of the robot. MOST consists of three angular rate sensors, three acceleration sensors, and a digital signal processor (DSP). The acceleration sensor is a semiconductor type detecting the mass displacement due to acceleration by the capacitance change. The angular rate sensor is a quartz type detecting a vibration change due to the Coriolis force by the charge change. The sensors are made by micro electro mechanical system (MEMS) technology and are used for automotive control in mass-produced automobiles. The set of posture angles is generally obtained by integrating angular rates over time. However, the posture angles diverge due to offset output integration. A new algorithm is proposed to suppress the divergence of the posture angles with the DSP in real time. The size and weight of MOST were 200 cm³ and 320 g, respectively. The accuracy of the posture angle was +/– 0.017 rad (+/– 1 deg). The sensing units enabled miniaturization and high reliability sufficient to meet long-term stability for the partner robot. Partner robots worked well for six months at the WORLD EXPO 2005 in Aichi, Japan. The highly reliable performance at the exhibition demonstrated that MOST is useful for posture-angle control of next-generation robots.

■KEYWORDS‖ Inertial Force, Posture Angles, Angular Rate Sensor, Acceleration Sensor, MEMS (Micro Electro Mechanical Systems) , Partner Robot, Human Support Robot, WORLD EXPO, Biped-type Robot, Rolling-type Robot

1. Introduction

The demands are many for robots throughout the world. In the production plants of automobile and electronics products, many kinds of robots are used for welding, painting, assembling, etc. At the present, the main usages of the robots are in the plants. They work in harsh environments in place of the workers and are completely isolated from these workers. In the plant, most automation robots are fixed on floors and the working areas are limited.

Another type of conventional robot is the rolling-type robot that has three, four, or six wheels. The bodies of conventional rolling robots are stable and move on the floor. They carry parts and assemblies of automobile and electronics products in the plant, but they cannot easily move fast and turn quickly on the floor.

People have high expectations for next-generation robots. They will be useful for nursing care, domestic help, office help, and personal assistance. They should be able to work with people and make contact with them as human support robots. Therefore, an autonomous control with a sensing system of their postures, a detecting system for objects and persons, and an evasive action system from the objects and persons are important for human support robots. Human support robots are free from anchors on the floor and move around people. That is one of the most important differences between conventional robots and next-generation ones.

Two types of robots, a biped-type and a rolling-type robot with two wheels, are representative of the next-generation robots, which work and move on the floor on feet or wheels. The biped-type robot can walk like a human with its legs and feet. The rolling-type robot has only two wheels, so it can turn quickly like a spindle and can run fast. The rolling-type robot with two wheels is an inverted pendulum type robot. The robot should be controlled to keep its balance in both stable and moving states. For the biped-type and the rolling-type robots with two wheels, detection of their posture or posture angles is

one of the required technologies. The robots can keep their postures and walk or run with their legs or wheels by using their posture or posture angle signals.

On the other hand, in the body control of humans, three semicircular canals are used to keep the body in good balance when a human stands up and walks with his legs or rides on wheels. If we can make an artificial semicircular canal and install it in the robots, the robots can stand up, walk and ride as a human does, as shown in **Fig. 1**. The biped-type robot can walk with its legs and feet as a human does when he walks with stilts, as shown on the left side of Fig. 1. The rolling-type robot can move as a human does when he rides a unicycle, as shown on the right side of Fig. 1. The three semicircular canals detect the angular rates of a human head and body. Gyro (angular rate) sensors also detect the angular rate in an artificial manner. Therefore, gyro sensors play a main role in the artificial semicircular canal, which is well known as an inertial sensing system.

"Partner robot" is our name for one of the human support robots. Typical applications of the partner robot are assistance for people, carrying goods and people, and personal mobility. The partner robot should walk and move freely around people and make contact with them to serve them. The partner robot can walk and move by using the inertial sensing system. However, no inertial sensing system is compact enough to be installed in the partner robots. We developed a new compact sensing system, called MOST (MOtion Sensing Technology), which works as the artificial semicircular canal in the partner robots. To make the artificial semicircular canal for the partner robots, the selection of the sensors such as an accelerometer and angular rate sensors is very important. As the sensors have to have a high degree of precision and be small

and reliable, the sensors for automobiles were selected. A new algorithm was developed to obtain a set of true posture angles in real time. This paper describes the sensors, the new algorithm, and MOST system to control the partner robot.

2. Theory

2. 1 Posture Angles

The posture angles of robots can be expressed in several ways. We use roll, pitch, and yaw systems with symbols ψ, θ, and ϕ. The standard coordinates of X, Y, and Z and the definitions of roll, pitch, and yaw are shown in **Fig. 2**. A posture matrix $\mathbf{T}(n)$ is expressed in Eq. (1). Rotation matrices for the roll, pitch, and yaw systems are described in Eqs. (2) to (4).

$$\mathbf{T}(n) = \begin{pmatrix} a & d & g & 0 \\ b & e & h & 0 \\ c & f & i & 0 \\ 0 & 0 & 0 & 1 \end{pmatrix} \tag{1}$$

$$\mathbf{RPY}(\phi,\theta,\psi) = \mathbf{Rot}(z,\phi) \cdot \mathbf{Rot}(y,\theta) \cdot \mathbf{Rot}(x,\psi) \tag{2}$$

$$\mathbf{RPY}(\phi,\theta,\psi) =$$
$$\begin{pmatrix} \cos\phi & -\sin\phi & 0 & 0 \\ \sin\phi & \cos\phi & 0 & 0 \\ 0 & 0 & 1 & 0 \\ 0 & 0 & 0 & 1 \end{pmatrix} \begin{pmatrix} \cos\theta & 0 & \sin\theta & 0 \\ 0 & 1 & 0 & 0 \\ -\sin\theta & 0 & \cos\theta & 0 \\ 0 & 0 & 0 & 1 \end{pmatrix} \begin{pmatrix} 1 & 0 & 0 & 0 \\ 0 & \cos\psi & -\sin\psi & 0 \\ 0 & \sin\psi & \cos\psi & 0 \\ 0 & 0 & 0 & 1 \end{pmatrix} \tag{3}$$

$$\mathbf{RPY}(\phi,\theta,\psi) =$$
$$\begin{pmatrix} \cos\phi\cos\theta & \cos\phi\sin\theta\sin\psi - \sin\phi\cos\psi & \cos\phi\sin\theta\cos\psi + \sin\phi\sin\psi & 0 \\ \sin\phi\cos\theta & \sin\phi\sin\theta\sin\psi + \cos\phi\cos\psi & \sin\phi\sin\theta\cos\psi - \cos\phi\sin\psi & 0 \\ -\sin\theta & \cos\theta\sin\psi & \cos\theta\cos\psi & 0 \\ 0 & 0 & 0 & 1 \end{pmatrix} \tag{4}$$
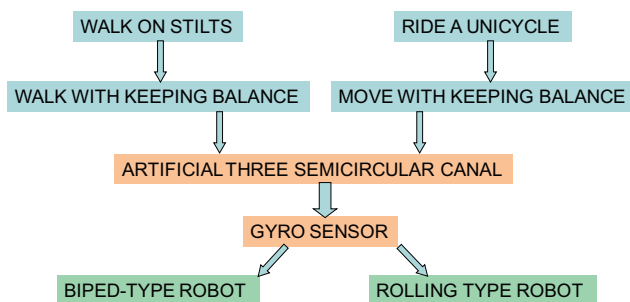
Fig. 1 Role of the artificial three semicircular canal.
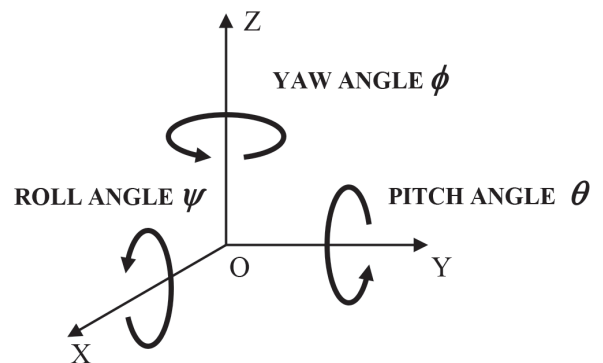
Fig. 2 Definition of roll, pitch, and yaw system.

When an angle δ is very small, $\sin\delta$ and $\cos\delta$ are approximated as in Eqs. (5) and (6). A minimal rotation matrix $\mathbf{A}(i)$ is obtained with minimal values of $\Delta\psi$, $\Delta\theta$, and $\Delta\phi$, as in Eq. (7). The values of $\Delta\psi$, $\Delta\theta$, and $\Delta\phi$ are obtained as Eqs. (8) to (10) with angular rates ω_x, ω_y, ω_z and sampling time t_s. In this case, the angular rates ω_x, ω_y, ω_z are obtained by the outputs of the three angular rate sensors. The minimal rotation matrix $\mathbf{A}(i)$ is obtained as Eq. (11). An initial posture matrix is $\mathbf{A}(0)$, as shown in **Fig. 3**. Then, a final posture matrix $\mathbf{T}(n)$ is obtained by postmultiplying the matrix $\mathbf{A}(0)$ by rotation matrices $\mathbf{A}(i)$ as in Eq. (12). The posture angles ψ, θ, and ϕ are derived from posture matrix elements as Eqs. (13) to (15). The variation ranges of the posture angles are shown in Eqs. (16) to (18).

Therefore, the posture angles ψ, θ, and ϕ are calculated from the outputs of the angular rate sensors.

Basically, the posture angles are obtained by integration of the angular rates in Eqs. (11) to (15). As the outputs of the angular rate sensors are not affected by accelerations, the posture angles obtained by the angular rate sensors are not affected by vibration accelerations while the robots walk and move. However, the posture angles obtained by the angular rates are divergent for a long period because offset outputs of the angular rate sensors are accumulated.

On the other hand, the posture angles are also obtained by measuring inclination angles to the gravity acceleration vector with the three acceleration sensors. **Figure 4** shows the relationship between

$$\sin\delta \approx \delta \tag{5}$$

$$\cos\delta \approx 1 \tag{6}$$

$$\mathbf{A}(i) = \begin{pmatrix} 1 & -\Delta\phi & \Delta\theta & 0 \\ \Delta\phi & 1 & -\Delta\psi & 0 \\ -\Delta\theta & \Delta\psi & 1 & 0 \\ 0 & 0 & 0 & 1 \end{pmatrix} \tag{7}$$

$$\Delta\psi = \omega_x \cdot t_s \tag{8}$$

$$\Delta\theta = \omega_y \cdot t_s \tag{9}$$

$$\Delta\phi = \omega_z \cdot t_s \tag{10}$$

$$\mathbf{A}(i) = \begin{pmatrix} 1 & -\omega_z \cdot t_s & \omega_y \cdot t_s & 0 \\ \omega_z \cdot t_s & 1 & -\omega_x \cdot t_s & 0 \\ -\omega_y \cdot t_s & \omega_x \cdot t_s & 1 & 0 \\ 0 & 0 & 0 & 1 \end{pmatrix} \tag{11}$$

$$\mathbf{T}(n) = \mathbf{A}(0)\mathbf{A}(1)....\mathbf{A}(n-1)\mathbf{A}(n) \tag{12}$$

$$\psi = \mathrm{atan2}\left(\sin\phi \cdot g - \cos\phi \cdot h, -\sin\phi \cdot d + \cos\phi \cdot e\right) \tag{13}$$

$$\theta = \mathrm{atan2}\left(-c, \cos\phi \cdot a + \sin\phi \cdot b\right) \tag{14}$$

$$\phi = \mathrm{atan2}\left(b, a\right) \tag{15}$$

$$-\pi < \psi \leq \pi \tag{16}$$

$$-\pi/2 \leq \theta \leq \pi/2 \tag{17}$$

$$-\pi < \phi \leq \pi \tag{18}$$
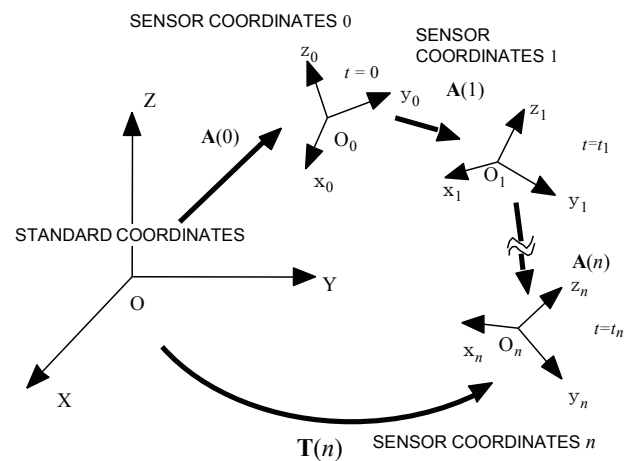
Fig. 3 Relationship between initial and final posture matrix.
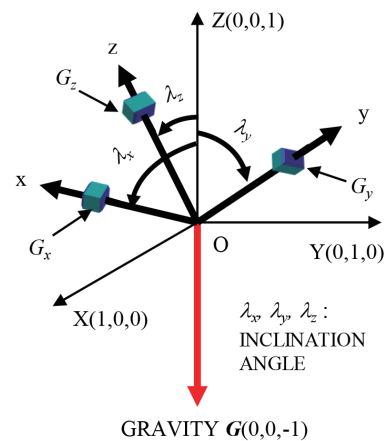
Fig. 4 Relationship between gravity and inclination angles.

the acceleration sensor alignment and the gravity acceleration. The sensor outputs of G_x, G_y, and G_z are normalized to G_x', G_y', and G_z' by Eqs. (19) to (21), and the inclination angles are shown by Eqs. (22) to (24).

$$G_x' = \frac{G_x}{\sqrt{G_x{}^2 + G_y{}^2 + G_z{}^2}} \qquad (19)$$

$$G_y' = \frac{G_y}{\sqrt{G_x{}^2 + G_y{}^2 + G_z{}^2}} \qquad (20)$$

$$G_z' = \frac{G_z}{\sqrt{G_x{}^2 + G_y{}^2 + G_z{}^2}} \qquad (21)$$

$$\lambda_x = \arccos\left(-G_x'\right) \qquad (22)$$

$$\lambda_y = \arccos\left(-G_y'\right) \qquad (23)$$

$$\lambda_z = \arccos\left(-G_z'\right) \qquad (24)$$

The posture angles obtained by the inclination angles are not divergent because the posture angles are derived from the accelerations directly without accumulation. However, the posture angles obtained by the accelerations are strongly influenced by translation and vibration accelerations while the robots walk and move.

These two kinds of posture angles obtained by the angular rate sensors and the acceleration sensors are combined to derive a complementary set of true posture angles.

2. 2 Algorithm

To suppress the divergence of the posture angle and to derive the true posture angle $\mathbf{Ptr}$, two kinds of posture angles, $\mathbf{Par}$ and $\mathbf{Pac}$, calculated from the angular rate and acceleration are used complementarily as shown in Eqs. (25) to (27). The posture angle $\mathbf{Par}$ from the angular rate consists of the true posture angle component $\mathbf{Ptr}$ and the drift component $\mathbf{Dar}$. The frequency spectrum of the drift component $\mathbf{Dar}$ is very low. The posture angle $\mathbf{Par}_{LPF}$ after application of a low pass filter (LPF) consists of a low-passed posture angle component $\mathbf{P}_{Low}$ and the drift component $\mathbf{Dar}$, as shown in Eqs. (28) to (30).

The posture angle $\mathbf{Pac}$ from the acceleration consists of the true posture angle $\mathbf{Ptr}$ and the noise component $\mathbf{Nac}$. The noise component $\mathbf{Nac}$ arises from translation and vibration acceleration. The frequency spectrum of

the noise component $\mathbf{Nac}$ is high. The posture angle $\mathbf{Pac}_{LPF}$ after the LPF consists of the low-passed posture angle component $\mathbf{P}_{Low}$.

The drift component $\mathbf{Dar}$ is obtained by subtracting the posture angle $\mathbf{Pac}_{LPF}$ from the posture angle $\mathbf{Par}_{LPF}$. Finally, the true posture angle $\mathbf{Ptr}$ is derived by subtracting the drift component $\mathbf{Dar}$ from the posture angle $\mathbf{Par}$, as shown in Eq. (31). MOST provides the true posture angle $\mathbf{Ptr}$ with high response and good stability by a feedback algorithm, as shown in **Fig. 5**.

$$\mathbf{Ptr} = \mathbf{P}_{High} + \mathbf{P}_{Low} \qquad (25)$$

$$\mathbf{Par} = \mathbf{Ptr} + \mathbf{Dar} = \mathbf{P}_{High} + \mathbf{P}_{Low} + \mathbf{Dar} \qquad (26)$$

$$\mathbf{Pac} = \mathbf{Ptr} + \mathbf{Nac} = \mathbf{P}_{High} + \mathbf{P}_{Low} + \mathbf{Nac} \qquad (27)$$

$$\mathbf{Par}_{LPF} = \mathbf{P}_{Low} + \mathbf{Dar} \qquad (28)$$

$$\mathbf{Pac}_{LPF} = \mathbf{P}_{Low} \qquad (29)$$

$$\mathbf{Dar} = \mathbf{Par}_{LPF} - \mathbf{Pac}_{Low} \qquad (30)$$

$$\mathbf{Ptr} = \mathbf{P}_{High} + \mathbf{P}_{Low} = \mathbf{Par} - \mathbf{Dar} = \mathbf{Par} - \left(\mathbf{Par}_{LPF} - \mathbf{Pac}_{LPF}\right) \quad (31)$$

$\mathbf{Ptr}$　True Posture Angle
$\mathbf{Par}$　Posture Angle from Angular Rate
$\mathbf{Pac}$　Posture Angle from Acceleration
$\mathbf{P}_{High}$　High Frequency Component of $\mathbf{Ptr}$
$\mathbf{P}_{Low}$　Low Frequency Component of $\mathbf{Ptr}$
$\mathbf{Dar}$　Drift Component of Posture Angle by Integration of Angular Rate (Response of $\mathbf{Dar}$ is low.)
$\mathbf{Nac}$　Noise Component of Posture Angle by Translation Acceleration (Response of the $\mathbf{Nac}$ is high.)
$\mathbf{Par}_{LPF}$　$\mathbf{Par}$ after LPF
$\mathbf{Pac}_{LPF}$　$\mathbf{Pac}$ after LPF

ψ, θ, ϕ : Posture Angle
PID: Proportional, Integral & Differential
LPF: Low Pass Filter
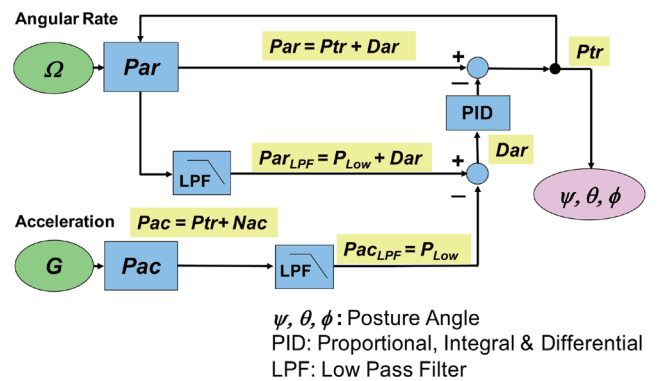
Fig. 5 Algorithm for divergent control.

Table 1   Comparison of various type angular rate (gyro) sensors.

TYPE	PRINCIPLE	SIZE	WEIGHT	ACCURACY	COST	OVERALL
RING LASER	SAGNAC EFFECT	LARGE	LARGE	EXCELLENT	EXPENSIVE	WRONG
OPTICAL FIBER	SAGNAC EFFECT	MEDIUM	MEDIUM	EXCELLENT	MEDIUM	GOOD
MECHANICAL	PRECESSION	MEDIUM	MEDIUM	GOOD	MEDIUM	GOOD
GAS RATE	CORIOLIS EFFECT	MEDIUM	MEDIUM	POOR	INEXPENSIVE	WRONG
VIBRATION	CORIOLIS EFFECT	SMALL	SMALL	GOOD	INEXPENSIVE	OPTIMUM

3. Structure of MOST

The key device of the sensing system is the angular rate sensor, which is usually called a gyro or rate gyro. The many kinds of angular rate sensors are shown in **Table 1**. The ring laser and the optical fiber types are optical types based on the Sagnac effect. They have good accuracy, but their sizes and weights are large and heavy. Moreover, their costs are high. The mechanical type with precession usually needs maintenance. The gas rate type is poor in accuracy for the posture angle measurement. The vibration type with the Coriolis effect is the optimum one for the robot, because its size and weight are small, its accuracy is relatively good, and its cost is low.

Based on the above-mentioned sensor characteristics, a vibration type of quartz detecting a vibration change due to the Coriolis force by a charge change was used for MOST. The quartz angular rate sensor is called a yaw rate sensor. It has been on-boarded in automobiles for detecting the yaw rates of an automobile.[1] The motion of an automobile is controlled safely with a vehicle stability control (VSC) system. The structure of the yaw rate sensor element is shown in **Fig. 6**. The element has an upper quartz fork for excitation and a lower quartz fork for detection. When the angular rate is applied to the sensor, the lower fork vibrates due to the Coriolis force. The lower fork only vibrates in applying the angular rate. **Figure 7** shows the electrodes on the quartz forks and the electrical interconnections. The sensor element mounted on an integrated circuit (IC) package is shown in **Fig. 8**. The size of the IC package is as small as $25 \times 25 \times 5$ mm. The small size is very important for installation in the robot.

On the other hand, the acceleration sensor used for MOST is a semiconductor type detecting a mass displacement due to acceleration by the capacitance change. The size of the acceleration sensor is small
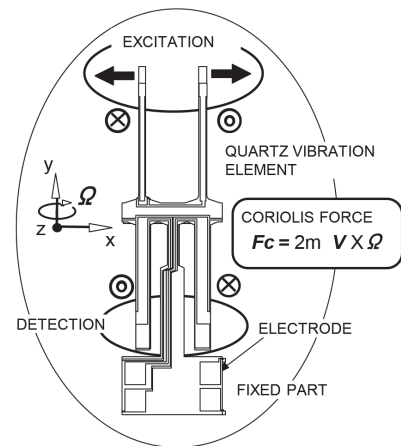
Fig. 6   Structure of the sensor element.
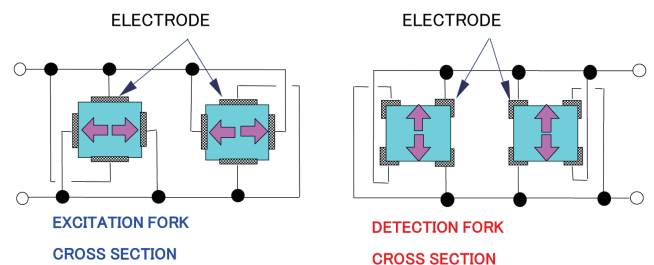
Fig. 7   Structure of the sensor electrodes and their connections.
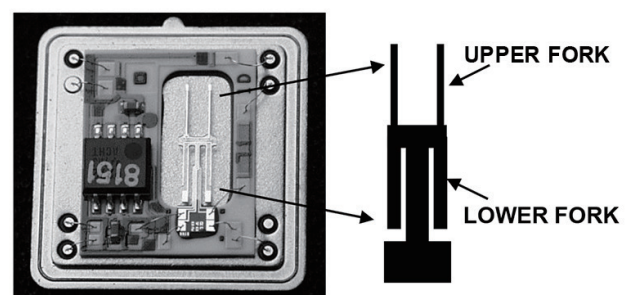
Fig. 8   Sensor element on the IC package, Package size: 25 mm L × 25 mm W × 5 mm H.

and it is also used in the VSC system.

The angular rate and acceleration sensors are made by micro electro mechanical systems (MEMS) technology. Since these sensors are used for controlling automobiles, they have high reliability over a wide temperature range and long-term durability. Such characteristics are considered to be quite important for highly reliable posture-angle control.

Then, the inertial force sensing system (MOST) consists of the above-mentioned three angular rate sensors, three acceleration sensors, and a digital signal processor (DSP), as shown in **Fig. 9**. The three angular rate sensors and the three acceleration sensors are arranged perpendicularly to each other. The temperature offset and sensitivity changes of the angular rate and acceleration sensors are compensated with the DSP. The misalignment of the perpendicular settings of the three sensors is compensated with a compensation matrix. The main role of the DSP is real-time calculation of the posture angles with the outputs of the angular rate and the acceleration sensors. It is all in one package, as shown in **Fig. 10**. The output signals of MOST are three axial posture angles, three axial angular rates, and three axial accelerations. The sensor signals are outputted with an RS232C digital communication interface. [2,3]

4. Results

MOST was evaluated on a three-axis stage. MOST was set up as the sensor coordinates parallel to the stage axes. The stage provided MOST with roll, pitch, and yaw motions independently. The stage oscillated MOST along the three axes like a tone burst wave.

One of the tone burst patterns was a three-axis rotation in phase, 5 times in 17 seconds and keeping still in 4 seconds. MOST was oscillated at the amplitude of $+/- 0.17$ rad ($+/- 10$ deg). This pattern simulated one of the robot walk patterns. In this case, the robot walked $5 + 5$ steps and rested, and walked. The posture angle outputs of MOST without the divergence suppression method are shown in **Fig. 11**. Each posture angle was changed according to the applied oscillation, but, in the still state, the posture angles of ψ, θ, and ϕ drifted and were divergent over time.

The posture angle outputs of MOST with the divergence suppression method are shown in **Fig. 12**. In the still state, the posture angles of ψ, θ, and ϕ did not drift over time. The three posture angles overlapped each other in this case. The drift of the posture angle of ϕ along the z direction was controlled to zero in this test.

The characteristics of MOST are listed in **Table 2**. The measurement ranges of the posture angles of ψ, θ, and ϕ were $+/- \pi$ rad ($+/- 180$ deg), $+/- \pi/2$ rad ($+/- 90$ deg), and $+/- \pi$ rad ($+/- 180$ deg), respectively. The angular rate range was $+/- 1.7$ rad/s ($+/- 100$ deg/s). The acceleration range was $+/- 1.5$ g. The attained accuracy of the posture angles of ψ and θ was $+/- 0.017$ rad ($+/- 1$ deg). The size of MOST was $5 \times 5 \times 8$ cm, and the volume was 200 cm³. The weight was as small as 320 g. The signals were outputted with the RS232C digital signal in a 10 ms period. The speed of the RS232C was 115 kbps.

MOST was installed in the partner robots, as shown in **Figs. 13** and **14**. The biped-type robots stood in a stable state, walked on their two legs and feet, and played the trumpet. The rolling-type robots stayed upright like an inverted pendulum and did not fall over. The rolling-type robots moved and spun with
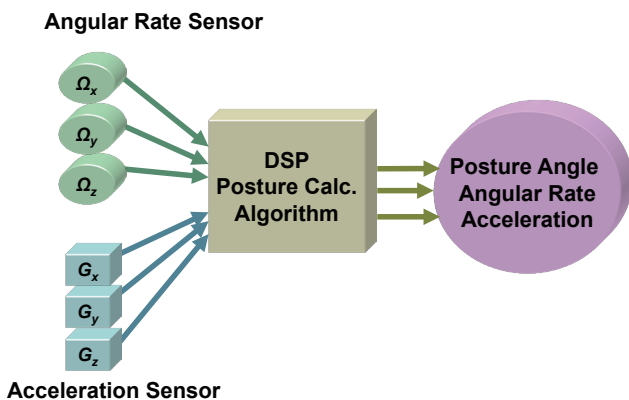
Fig. 9 Block diagram of the inertial force sensing system.
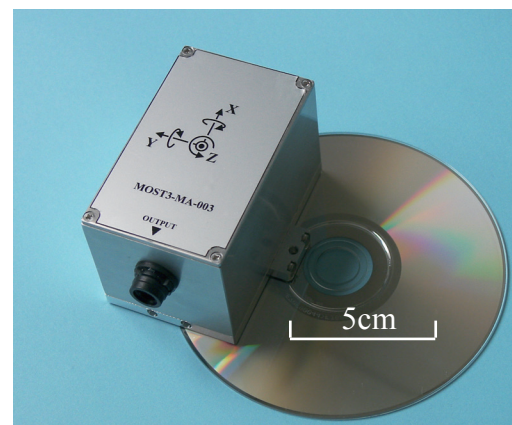
Fig. 10 Photograph of MOST.

their wheels on the floor and played the trumpet, too. The biped-type robot with a wire drive had feet driven with wires. The wire-driven feet were light and walked lightly, like birds' feet. The person carrier biped-type robot also had two legs and feet. A person actually got on board and walked with the feet of the robot. MOSTs were on-boarded in all of the robots in the TOYOTA group pavilion at the WORLD EXPO 2005 in Aichi, Japan.[4] They walked and moved stably and safely with good balance, because they were controlled with MOSTs. MOSTs, serving as artificial semicircular canals, worked well. The partner robots with MOSTs demonstrated good actions and sounds all day long for six months at the exhibition.

5. Discussion

The acceleration and angular rate sensors in MOST were the product sensors used for the VSC system in an automobile. An automobile runs and turns stably at curves and on wet and snowy roads due to help of the VSC. The working ranges of the acceleration and angular rate sensors for the robots were similar to the

range for automobile use. Therefore, the automobile sensors were utilized for robot control without any difficulties. As the size of MOST was compact with the small automobile sensors and the DSP chip, all of the robots were mounted with MOST and showed good performance.

The acceleration and angular rate sensors were single-axis type sensors. Three-axis sensor setups for detecting three-axis acceleration and angular rate were made by orthogonal placement of the sensors to each other. Temperature compensations of the sensor outputs were made with a temperature sensor in MOST housing and the DSP.

Table 2 The characteristics of MOST.

	ITEM		RANGE
SENSOR	ANGULAR RATE	3	
	ACCELERATION	3	
DSP		1	
OUTPUT	POSTURE ANGLE	3	ψ +/- π rad (+/- 180 deg)
			θ +/- π / 2 rad (+/- 90 deg)
			ϕ +/- π rad (+/- 180 deg)
	ANGULAR RATE	3	+/- 1.7 rad/s (+/- 100 deg/s)
	ACCELERATION	3	+/- 1.5 g
	TEMPERATURE	1	- 40 to 80 degC
	DIGITAL RS232C	1	115 kbps
	ANALOG	(3)	0 to 5 V
	ACCURACY (ψ, θ)		+/- 0.017 rad (+/- 1 deg)
UNIT	SIZE		5 W, 5 H, 8 D cm
	VOLUME		200 cm^3
	WEIGHT		320 g
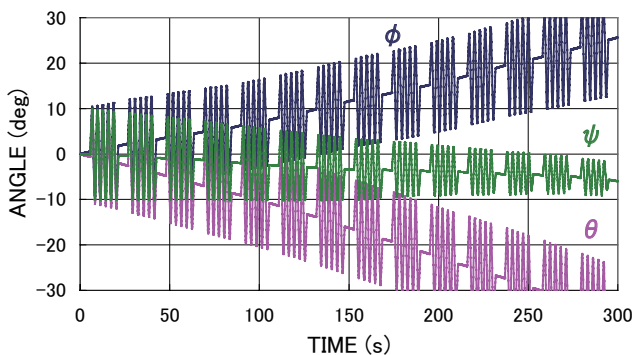
Fig. 11 Posture angle outputs with no divergent suppression.
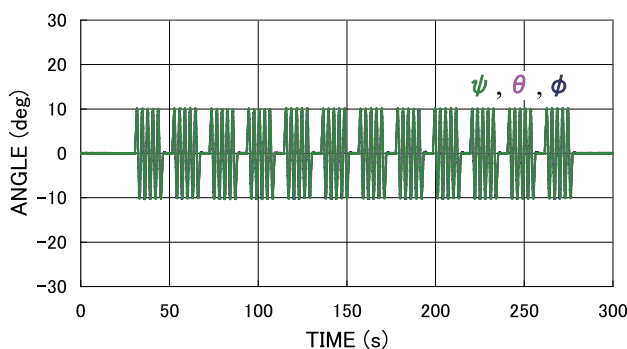
Fig. 12 Posture angle outputs with divergent suppression.
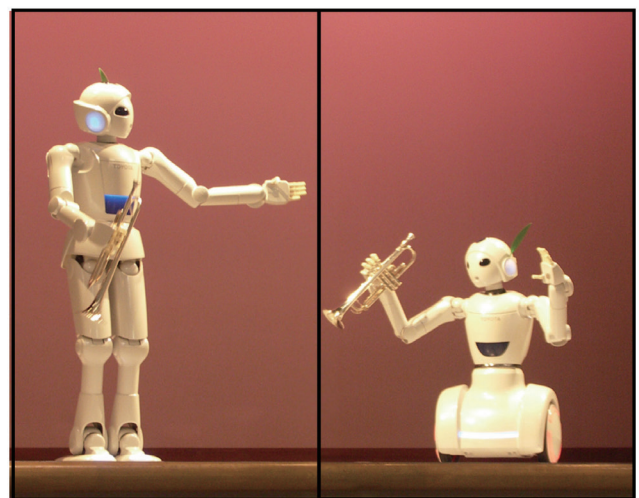
Fig. 13 Partner robots with MOST, biped-type (left) and rolling-type (right).

Parson carrier biped-type robot

Biped-type robot

Biped-type robot with wire drive

Rolling-type (2 wheels) robot

5cm
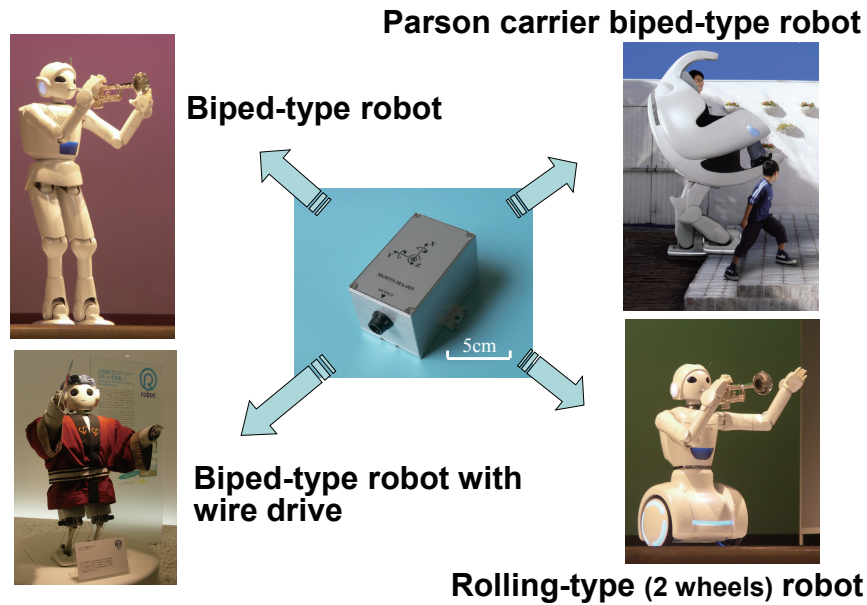
Fig. 14 Partner robot family with MOST shown in Aichi Expo 2005.

The algorithm for MOST system was made with the proportional-integral-derivative (PID) algorithm instead of the commonly used Kalman filter. It was difficult to understand the Kalman filter coefficient effects as physical images. However, it was easy to obtain pictures of the PID parameter effects. A PID system was developed for the posture angle domain, in which the values of the posture angles were cyclic, not linear. This was one of the important points for the PID system with posture-angle control. The adjustments of the PID parameters were made successfully by MOST parameter tunings on actual robots.

MOST provided zero stability in the posture angle that made the robots able to stand up in stable condition. MOST also provided reliability that allowed active performances for a long time. As a good example, MOST was useful for detecting the posture and posture angles, and controlling the robots and moving machines.

of the partner robots.

One set of posture angles for the robots was obtained from the angular rate sensors. Another set of posture angles was also obtained from the acceleration sensors. A set of true posture angles was calculated by the DSP by using the two sets of posture angles from the angular rate sensors and the acceleration sensors complementarily. A new algorithm was developed and successfully suppressed the divergence of the posture angles over time.

The system was called MOST. The size and weight of MOST were as small as 200 cm^3 and 320 g, respectively. The accuracy of the posture angle was +/– 0.017 rad (+/– 1 deg). These dimensions and accuracy were good for installation in partner robots. Partner robots worked well for six months at the WORLD EXPO 2005 in Aichi, Japan. The highly reliable performance at the exhibition demonstrated that MOST is useful for posture-angle control of next-generation robots.

6. Conclusions

An inertial force sensing system was developed for partner robot use. The system consists of three acceleration sensors, three angular rate sensors and a DSP. The angular rate sensor, known as a gyro sensor, played an important role. The angular rate sensor was made of quartz and is used in automobiles. It was suitable for reduction in size and weight in the system

References

(1) Nonomura, Y., Fujiyoshi, M., Omura, Y., Tsukada, K., Okuwa, M., Morikawa, T., Sugitani, N., Satou, S., Kurata, N. and Matsushige, S., "Quartz Rate Gyro Sensor for Automotive Control", *Sensors & Actuators A,* Vol. 110 (2004), pp. 136-141.

(2) Nonomura, Y., Fujiyoshi, M. and Sugihara, H., "Development of Inertial Force Sensing System for

Partner Robots", *Proceedings of the 23rd Sensor Symposium* (2006), pp. 55-59.

(3) Nonomura, Y., Fujiyoshi, M., Sugihara, H., "Inertial Force Sensing System for Partner Robots", *IEEE SENSORS 2006* (2006) , pp. 1325-1328.

(4) TOYOTA MOTOR CORP, "TOYOTA. CO. JP -NEWS RELEASE-" <http//:www.toyota.co.jp/en/news/04/1203_1d.html>, (2005), (accessed 2014-05-20).

Figs. 1-4, 6-7, 9-13 and Table 2
Partially reprinted and modified from Proceedings of the 23rd Sensor Symposium (2006), pp. 55-59, Nonomura, Y., Fujiyoshi, M. and Sugihara, H., Development of Inertial Force Sensing System for Partner Robots, © 2006 The Institute of Electrical Engineers of Japan, with permission from the Institute of Electrical Engineers of Japan.

Figs. 5 and 8
Reprinted from IEEE SENSORS, (2006), pp. 1325-1328, Nonomura, Y., Fujiyoshi, M. and Sugihara, H., Inertial Force Sensing System for Partner Robots, © 2006 IEEE, with permission from IEEE.

Yutaka Nonomura
  Research Fields:
    - Sensors for Automobiles
    - MEMS (Micro Electro Mechanical Systems)
  Academic Degree: Dr.Eng.
  Academic Societies:
    - The Magnetics Society of Japan
    - The Japan Society of Applied Physics
    - The Institute of Electrical Engineers of Japan
    - IEEE
  Award:
    - Outstanding Paper Award at Transducers '11, 2011

Motohiro Fujiyoshi
  Research Field:
    - MEMS Sensor
  Academic Degree: Dr.Eng.
  Academic Societies:
    - IEEE
    - The Institute of Electrical Engineers of Japan
  Award:
    - Outstanding Paper Award at Transducers '11, 2011
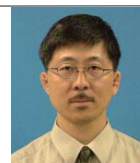
Hisayoshi Sugihara*
  Research Field:
    - Development of Personal Mobility
  Academic Societies:
    - The Japan Society of Mechanical Engineers
    - The Robotics Society of Japan

*TOYOTA MOTOR CORPORATION